文章编号：1001－9014(2016)03－0267－05

DOI:10.11972/j.issn.1001－9014.2016.03.003

A broad stop-band filter based on multilayer metamaterials in the THz regime

ZHANG Li-Hua[1,2], LI Ji-Jun[3*], BAO Yu-Hai[1], WANG An-Xiang[4], ZHANG Wei-Guang[3]

(1. Inner Mongolia Autonmous Region Key Laboratory of Geographic Information System and Remote Sensing, Inner Mongolia Normal University, Hohhot 010022, China;
2. College of Water Science, Beijing Normal University, Beijing 100875, China;
3. College of Science, Inner Mongolia University of Technology, Hohhot 010051, China;
4. School of Science, Xi'an Polytechnic University, Xi'an 710048, China)

Abstract: A periodic multilayer structure of metal and dielectric layer has been proposed and studied to gain a stop-band filter in the THz range. A broad stop-band has been realized through making use of polarization hybridization. The bandwidth of the stop-band filter can be tunable in a large range through electric-magnetic couplings in silver layers. The influences of the number of metal layer, the lattice constant and the permittivity of dielectric layer on the central frequency and stop-bandwidth have been studied. The central frequency would be blue-shifted and stop-bandwidth can be expanded through selecting these parameters appropriately. The bandwidth tunability which can be worked through the coupling effect provides good guidance for designing broad stop-band filter.

Key words: filter, metamaterials, resonance mode, stop-band, polarization hybridization
PACS: 41. 20. Jb, 78. 20. Cj, 73. 20. Mf, 42. 25. Bs

一种太赫兹频段的大带宽多层超材料阻带滤波器

张丽华[1,2], 李继军[3*], 包玉海[1], 王安祥[4], 张伟光[3]

(1. 内蒙古师范大学, 内蒙古自治区遥感与地理信息系统重点实验室,内蒙古 呼和浩特 010022;
2. 北京师范大学水科学研究院, 北京 100875;
3. 内蒙古工业大学理学院, 内蒙古 呼和浩特 010051;
4. 西安工程大学理学院,陕西 西安 710048)

摘要:设计并研究了一种周期性多层金属/介质层结构以获得太赫兹频段的阻带滤波器.通过利用极化综合效应实现了一个大带宽的阻带.这一阻带滤波器的带宽可以通过调制银层的电磁耦合作用进行调节.同时还研究了金属层的数量、晶格常数和介质层的介电常数对阻带滤波器的中心频率和带宽的影响.通过合理调配这些因素可以调制中心频率蓝移和带宽增大.通过耦合作用调制带宽的方法可为设计大带宽阻带滤波器提供好的思路.

关 键 词:滤波器;超材料;共振模式;阻带;极化综合

中图分类号:O431 **文献标识码**:A

Introduction

Metamaterials have attracted enormous researchers' interest in recent years because of their unique electromagnetic properties available in natural materials[1]. Metamaterials can be made up of structural metallic and dielectric layers, either supported by a suitable substrate or free standing. Many species of unit cells based on metamaterials have been proposed during the past few years, such as cut-wire pairs [2] and metallic split ring resonators [3]. More and more optical devices based on

Received date: 2015 - 09 - 30, **revised date**: 2015 - 12 - 16 **收稿日期**:2015 - 09 - 30, **修回日期**:2015 - 12 - 16
Foundation items:Supposted by the National Natural Science Foundation of China (11562016), the Natural Science Foundation of Inner Mongolia Autonomous Region (2016Ms0408,2013MS0107), the College Science Research of Inner Mongolia Autonomous Region (NJZZ16041), and the Scientific Research Foundation for the High-level Talents of Inner Mongolia Normal University (2014YJRC022)
Biography:ZHANG Li-Hua(1979-), female, Hohhot, China, associate professor, Ph. D. Research fields focus on remote sensing physics.
* **Corresponding author**:E-mail:dapperzhanglh@163.com

metamaterials have been investigated, such as perfect absorbers[4], perfect lens [5], imaging [6], and filters [7-8]. Recently, some researchers have been focused on the THz stop-band filter which is designed to filter specific frequencies of wave propagating and ensure high tolerances well to frequency operations in the THz range[9]. However, many stop-band filters do not work well in eliminating the interfering signals or suppression of undesired responses in the THz region. The resonant stop-band is always too narrow, which significantly limits these filters application in filtering broadband radiation. The resonant nature of these structural stop-band filters leads to the appearance of several resonant dips in the stop-band, and thus results reduction of the stop-bandwidth. It is important to design and provide a broad stop-band filter with few resonant dips in stop-band. Moreover, the designed stop-band filter can be fabricated practical, with high-efficiency broad stop-band. Motivated by these reasons discussed above, a Square-Ring-Square-Patch structure (SRSP) has been designed in this paper. The stop-bandwidth and central frequency of the filter is tunable by adjusting the number of metal layer, the lattice constant and the permittivity of dielectric layer. Moreover, resonance modes in the stop-band interact and couple together, which means that the stop-bandwidth of filter can be expanded by adjusting these factors without worrying about the appearing of new resonance dips. The filter can be designed to select stop-bandwidth in the THz regime and can be manufactured practically.

1 Structures and Design

A unit cell of a SRSP structure was designed in this paper as the basic microstructure of stop-band filter, as illustrates in Fig. 1. The multilayer microstructure consists of one dielectric layer and two silver layers. Silver layers are separated by the dielectric layer. Each silver layer is perforated with an array of square-loop-cross-shaped metal strips. The chosen strip pattern is a symmetric and simple structure, which exhibits excellent low transmission. The dielectric layer is selected as SU-8 in simulation. The dimensional parameters are: $P = 20$ μm, $L1 = 18$ μm, $L2 = 12$ μm, $L3 = 4$ μm, $h1 = 0.2$ μm, $h2 = 5$ μm. The SRSP structure with these dimensions can be fabricated in practice through electron-beam lithography or focus-ion-beam milling[10].

The commercial software Ansoft HFSS13.0 was employed to find the potential physics behind the transmittance band. The electric field is in the y axis (E) and the magnetic field is in the x axis (H). The polarized wave propagates along the z axis (k). In simulation, two ideal electric conductor planes have been used on the boundary normal to the y axis and two ideal magnetic conductor planes has been utilized on the boundary normal to the x axis[11]. The dielectric constant of SU-8 is $2.56 + 0.035i$[12] and the Drude model is used to describe the dielectric constant of the silver layer:

$$\varepsilon(\omega) = 1 - \frac{\omega_p^2}{\omega^2 - i\omega\gamma_D} \quad , \quad (1)$$

here, $\omega_p = 1.37 \times 10^{16}$ s^{-1} is the plasma frequency and $\gamma_D = 9 \times 10^{13}$ s^{-1} is the collision frequency [13], respectively.

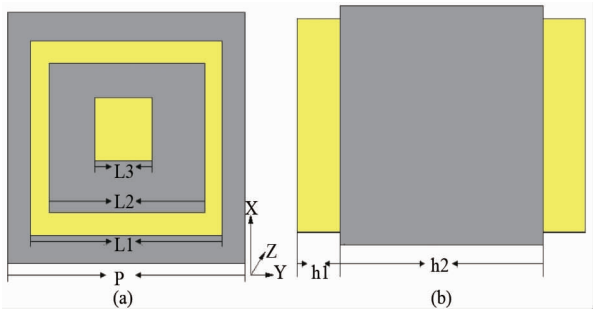

Fig. 1 (a) The top view of a unit cell; (b) the side view of a unit cell for $n = 2$. The yellow part is silver layer, and the gray part is dielectric layer

图1 (a) 晶胞顶视图;(b) 晶胞侧视图($n = 2$). 其中黄色部分为银层,灰色部分为介质层

2 Simulated results

Simulated results with different number of silver layers (n) are shown in Fig. 2. A stop-band appears in the transmission spectra with n increasing. Figure 2 (a) shows the simulated transmission with the unit cell of a single silver layer and a single SU-8 layer. The stop-band dip locates at $f_0 \approx 4.82$ THz, which corresponds to a single resonance dip and the stop-bandwidth is $\Delta f \approx 0.31$ THz. In this paper, the stop-bandwidth is defined as $\Delta f = (f_{high} - f_{low})$, and the central frequency is defined as $f_{cen} = (f_{low} + f_{high})/2$ (the f_{low} is defined as the lower-frequency point at which 4% energy transmits through the SRSP structure and the f_{high} is defined as the higher-frequency point at which 4% energy transmits). A typical stop-band filter can be obtained through stacking a silver layer and a SU-8 layer. However, the bandwidth is too narrow to be used for filtering broadband radiation effectively. In order to expand the stop-bandwidth, the n is increased. For $n = 2$, the stop-band dip is expanded to $\Delta f \approx 3.92$ THz. The central frequency is locates at $f_0 \approx 5.08$ THz. A typical broad stop-band filter has been obtained by increasing the number of silver layer. This means that the designed structure is valid. The expanded stop-bandwidth and the blue-shifted of the central frequency is consistent in the case of $n = 3$, $n = 4$, $n = 5$, see the dashed line. The result in Fig. 3 reveals that the value of n has an important influence on the property of the filter.

3 Discussion for SRSP structure filter

Recently, many researchers focus on exploring the interaction between wave and periodical structures[14]. To gain insight into the mechanism which leads to the broad stop-band, the resonance modes for $n = 3$ has been investigated in the near-field. At the resonance frequency $f_0 \approx 5.5$ THz, the distribution of electric field is similar in each layer. The resonance intensity is obviously decreased from the top to the underneath layer, as illustrated in Fig. 4 (a-c). To study the resonance modes in

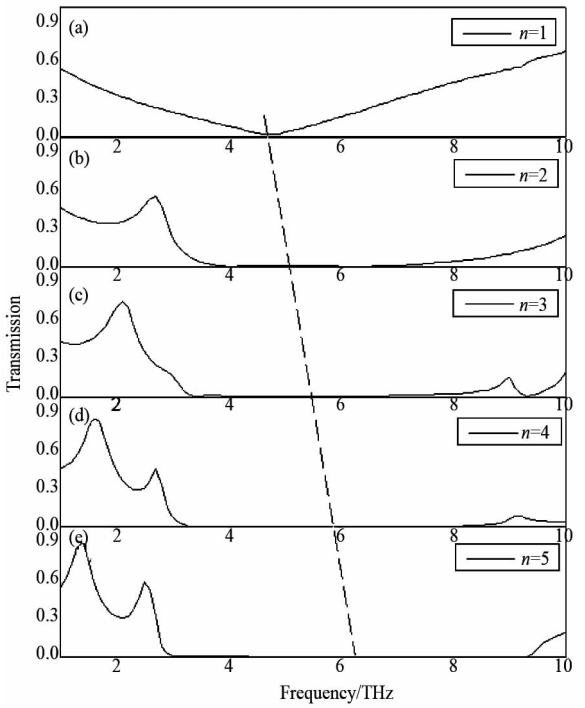

Fig. 2　Simulated transmittance spectra of filter with different number of silver layers: (a) $n=1$; (b) $n=2$; (c) $n=3$; (d) $n=4$; (e) $n=5$

图 2　不同银层数的滤波器的模拟透射谱: (a) $n=1$; (b) $n=2$; (c) $n=3$; (d) $n=4$; (e) $n=5$

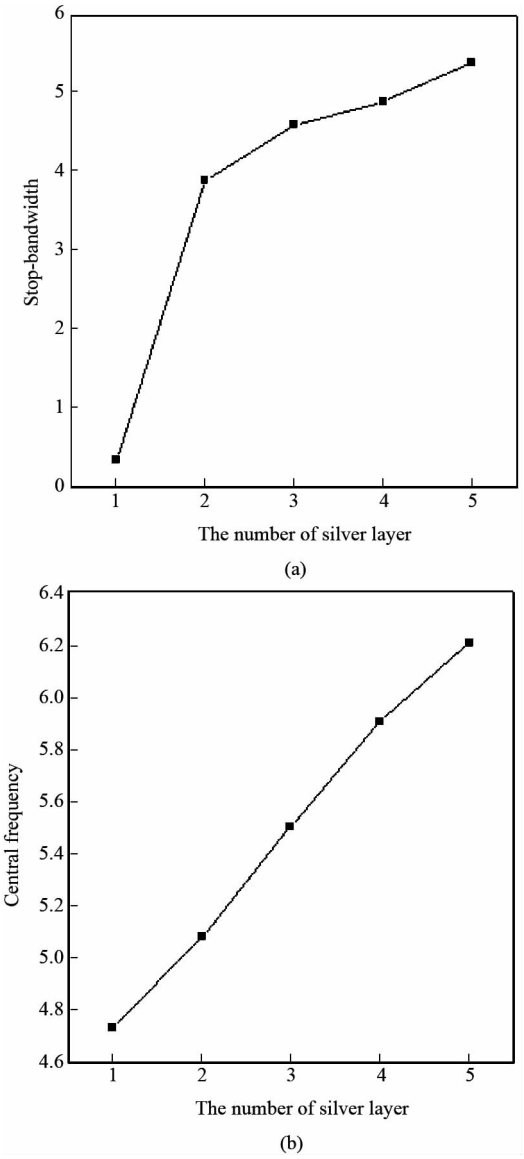

Fig. 3　(a) Stop-bandwidth of filter with different number of silver layers: (a) $n=1$; (b) $n=2$; (c) $n=3$; (d) $n=4$; (e) $n=5$; (b) Central frequency of filter with different number of silver layers: (a) $n=1$; (b) $n=2$; (c) $n=3$; (d) $n=4$; (e) $n=5$

图 3　(a) 不同银层数的滤波器对应的阻带宽度: (a) $n=1$; (b) $n=2$; (c) $n=3$; (d) $n=4$; (e) $n=5$; (b) 不同银层数的滤波器的中心频率: (a) $n=1$; (b) $n=2$; (c) $n=3$; (d) $n=4$; (e) $n=5$

Fig. 4(a), different frequency have been selected for investigating the distribution of the resonance mode. On the one hand, when the frequency is low, such as $f_0=2$ THz, the resonance mode exhibits a strong coupling between two adjacent unit cells, as shown in Fig. 4(d). On the other hand, when the frequency is high, such as $f_0=9$ THz, the resonance mode reveals inward coupling between the Square-Ring and the Square-Patch, as shown in Fig. 4(f). It can be found that when the resonance frequency is out of the stop-band range, there is only one resonance mode. Finally, when the frequency is within the stop-band range, such as $f_0=5.5$ THz, the two resonance modes in each plane start to interact and couple together and thus produces the plasmonic hybridization, as shown in Fig. 4(e). It is obvious that both of the two hybridized resonance modes are strong. The transmission out of the stop-band is higher than 0.25 with the dielectric loss, as shown in Fig. 2(c). It is the same as the transmission within the stop-band range. However, the enhanced electric resistance caused by the polarization hybridization in the stop-band range also decreases the transmission too. It can be found that the lateral plasmonic hybridization is the main reason which leads to the broad stop-band.

In fact, in addition to the number of silver layers, the variation of permittivity of dielectric layer and lattice constant have great effects on the optical response of the stop-band filter. In the following, the effects of these two parameters are investigated. To illustrate interaction between adjacent unit cells, the transmission spectra of different lattice constant for $n=3$ are plotted in Fig. 6. The stop-bandwidth is increased from $\Delta f\approx 3.05$ THz to $\Delta f\approx 4.6$ THz with lattice constant reducing. On the other hand, the permittivity of dielectric layer has been decreased from $\varepsilon=3$ to $\varepsilon=1.5$, as shown in Fig. 7. It can be found that the primary effect of varying the dielectric is to blue-sifted the central frequency and stop-band broadened. Moreover, the multilayer electron-beam lithography technique can be used to manufacture the SR-SP structure [10]. It means that the fabrication of CRR structure filter is feasible and practical.

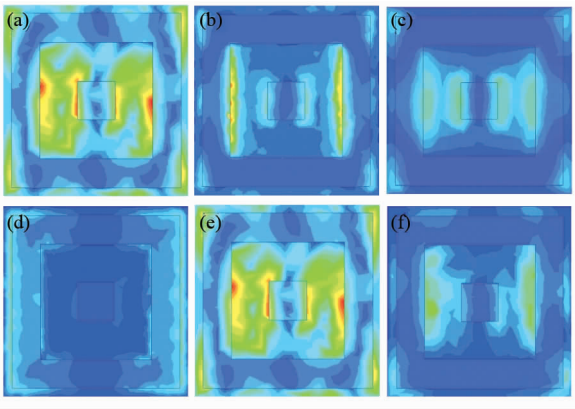

Fig. 4 (a) ~ (c) Simulated distributions of the electric field in the top, middle, and underneath layers at f_0 = 5.5 THz, respectively. (d) ~ (e) Simulated distributions of the electric field in the top layer of CRR structure at frequencies of 2, 5.5, and 9 THz, respectively.

图4 (a) ~ (c)谐振频率为5.5 THz时在顶层、中间层和底层金属层上的电场分布的模拟结果;(d) ~ (e) 谐振频率为2,5.5,9 THZ时顶层CRR结构超材料上的电场分布的模拟结果

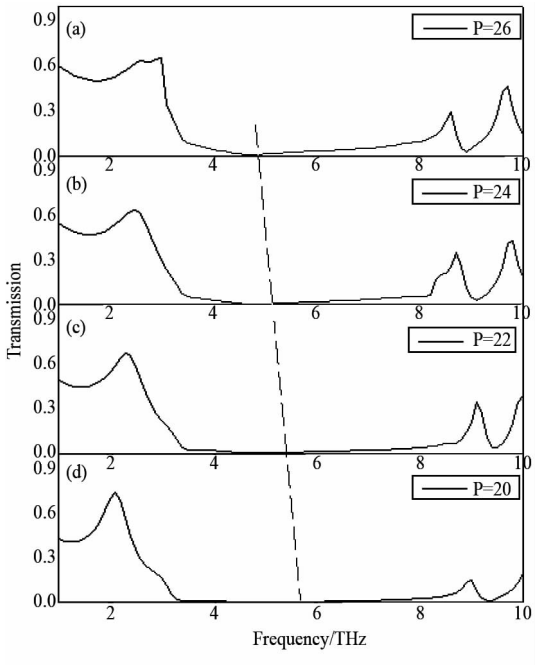

Fig. 5 Simulated transmission spectra of different lattice constant with n = 3

图5 不同晶格常数的模拟透射谱(n = 3)

4 Conclusions

A broad stop-band filter has been designed, simulated, and explained in the THz regime. Results indicate that a broad stop-band filter can be realized by stacking layers of silver layers and SU-8 layers. The stop-band-width and central frequency can be tunable by adjusting the number of metal layers, the lattice constant and the permittivity of dielectric layer. The mechanism behind the stop-band is the plasmonic hybridization of adjacent unit cells coupling resonance mode and inward coupling mode, which would prohibit appearing of new resonance dips. The stability in the stop-band transmission response of the SRSP structure filter enables its use in many THz optical devices.

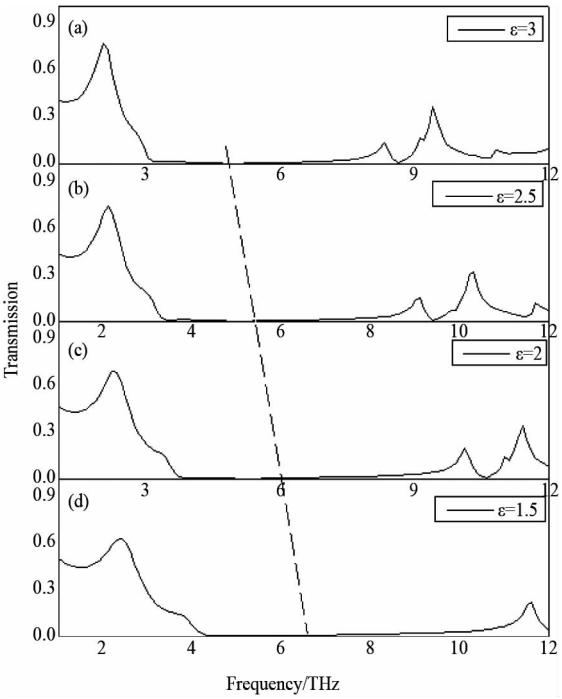

Fig. 6 Simulated transmission spectra of different dielectric constant with n = 3

图6 不同介电常数的模拟透射谱(n = 3)

Acknowledgments

This research is supported by the National Natural Science Foundation of China (Grant No. 11562016), the Natural Science Foundation of Inner Mongolia Autonomous Region (Grant No. 2016MS0408 and 2013MS0107), the College Science Research of Inner Mongolia Autonomous Region (Grant No. NJZZ16041), and the Scientific Research Foundation for the High-level Talents of Inner Mongolia Normal University (Grant No. 2014YJRC022).

References

[1] Pendry J B, Holden A J, Robbins D J, *et al*. Magnetism from conductors and enhanced nonlinear phenomena[J]. *IEEE Trans. Microw. Theory Tech*, 1999, **47**(11): 20752084 - 20752088.

[2] Shalaev V M, Cai W, Chettiar U K, *et al*. Negative index of refraction in optical metamaterials[J]. Opt. Lett, 2005, **30**(24): 33563356 - 33563358.

[3] Shelby R A, Smith D R, Schultz S. Experimental verification of a negative index of refraction[J]. Science, 2001, **292**(5514): 77 - 79, 2001.

[4] Alaee R, Farhat M, Rockstuhl C, *et al*. A perfect absorber made of a grapheme micro-ribbon metamaterial[J]. Optics Express, 2012, **20**: 28017 - 28024.

(下转第349页)

[2] Inter-calibration of geostationary (GOES, METEOSAT, GMS) and polar-orbiting (HIRS and AVHRR) infrared window radiances[R]. CGMS-XXVII-USA-WP-21, 13-19 October 1999 in Beijing, China.
[3] Konig M. Tjemkes S, Hans-Joachim Lutz. The importance of using clear radiances and near-nadir views for satellite intercalibration[R]. CGMS-XXVIII EUM-WP-16, 16-20 October 2000 in Woods Hole, MA, USA.
[4] Tobin DC, Revercomb H E, Moeller C C, *et al*, 2006: Use of at mospheric infrared sounder high-spectral resolution spectra to assess the calibration of moderate re solution imaging spectroradiometer on EOS aqua [J], *J. Geophys. Res.*, 111, D09S05, doi:10.1029/2005JD006 095.
[5] Gunshor M M, Schmit T JMenzel, W P, *et al*, Intercalibration of broadband geostationary imagers using AIRS[J]. *J. Atmos. Oceanic Technol*. 2009, **26**:746 - 758.
[6] Cao C, Goldberg M, Wang L. Spectral bias estimation of historical HIRS using IASI observations for improved fundamental climate data records[J]. *J. Atmos. Oceanic Technol*, 2009, **26**(7): 1378 - 1387.
[7] Wang L, Goldberg M, Wu X, *et al*. Consistency assessment of atmospheric infrared sounder and infrared atmospheric sounding interferometer radiances: double differences versus simultaneous nadir overpasses [J]. *J. Geophys. Res.*, 2011, **116**:D1111.
[8] Xu Na, Hu Xiu-Qing, Chen L, *et al*. Inter-calibration of infrared channels of FY-2/VISSR using high-spectral resolution sensors IASI and AIRS[J]. *J. Remote Sensing*(徐娜, 胡秀清, 陈林等, FY-2 静止卫星红外通道的高光谱交叉定标, **遥感学报**), 2012, **16**(5): 939 - 952.
[9] Zhang Y, Gunshor M M. Intercalibration of FY-2C/D/E infrared channels using AIRS[J]. *IEEE Transactions on Geoscience and Remote Sensing*, 2013, **51**(3): 1231 - 1244.
[10] HU Xiu-qing, XU Na, WENG Fu-zhong, ZHANG Yong. Long-term monitoring and correction of FY-2 infrared channel calibration using AIRS and IASI[J]. *IEEE Transactions on Geoscience and Remote Sensing*, 2013, **51**(10): 5008 - 5018.
[11] Wang L, Cao C, Goldberg M. Intercalibration of GOES-11 and GOES-12 water vapor channels with MetOp IASI hyperspectral measurements[J]. *Journal of Atmospheric and Oceanic Technology*, 2009, **26**:1843 - 1855.
[12] Yu F, Wu X, Radiometric calibration accuracy of GOES sounder infrared channels[J]. *IEEE Transactions on Geoscience and Remote Sensing*, 2013, **51**(3):1187 - 1199.
[13] Hewison T J. An evaluation of uncertainy of the GSICS SEVIRI-IASI intercalibration products[J]. *IEEE Transactions on Geoscience and Remote Sensing*, 2013, **51**(3):1171 - 1181.
[14] Hewison T J. Ice contamination of meteosat/SEVIRI implied by intercalibraion against metop/IASI [J]. *IEEE Transactions on Geoscience and Remote Sensing*, 2013, **51**(3):1182 - 1186.
[15] Yoshihiko T. New spectral compensation method for intercalibraion using high spectral resolution sounder[R]. Meteorological Satellite Center Technical Note, 2008, **50**:1.
[16] XU Na, HU Xiu-qing, CHEN Lin, *et al*. On-orbit radiometric calibration accuracy of FY-3A MERSI thermal infrared channel[J]. *Spectroscopy and Spectral Analysis*(徐娜, 胡秀清, 陈林等, FY-3A/MERSI 热红外通道在轨辐射定标精度评估, **光谱学与光谱分析**), 2014, **34**(12):3429 - 3434.
[17] XU Han-lie, XU Na, HU Xiu-qing. Inter-calibration of infrared bands of FY-3C MERSI and VIRR using hyperspectral sensor CrIS and IASI[C]. 2014, ASIA-PACIFIC REMOTE SENSING Proc. SPIE, 9264 - 10.
[18] QI Cheng-Li, HU Xiu-Qing, ZHANG Li-Yang, *et al*. 2012. Cross-calibration of FY1C/1D satellite based on hyper-spectral data[J]. *Acta Meteorologica Sinica*(漆成莉, 胡秀清, 张里阳等, 基于高光谱资料对 FY-1 气象卫星进行交叉定标, **气象学报**), 2012, **70**(4):892 - 901.
[19] RONG Zhi-Guo, ZHANG Yu-Xiang, LU Feng, *et al*. Inter calibration of FY-2B IR channel with NOAA satellites [J]. *Acta Meteorologica*(戎志国, 张玉香, 陆风, 等, FY-2B 与 NOAA 卫星红外通道的相对定标, **气象学报**), 2005, **63**(4):485 - 492.
[20] QI Cheng-li, XU Han-lie, YIN De-kui. FY3C IRAS on-orbit performance and measurements validation, ASIA-PACIFIC REMOTE SENSING Proc[C]. 2014, SPIE, 9264 - 8.
[21] MittazJ P D, Harris, A R, Sullivan J T., A physical method for the calibration of AVHRR/3 thermal IR channels 1: The prelaunch calibration data[J]. *Atmos. Ocean. Technol.*, 2009, **26**(9): 996 - 1019.

(上接 270 页)

[5] Fang N, Lee H, Sun C, *et al*. Sub-Diffraction-Limited Optical Imaging with a Silver Superlens[J]. Science, 2005, **308**: 534 - 537.
[6] Schuring D, Mock J J, Justice B J, *et al*. Metamaterial Electromagnetic Cloak at Microwave Frequencies[J]. Science, 2006, **314**: 977 - 981.
[7] Garcia-Garcia J, Bonache J, Gil I, *et al*. Miniaturized microstrip and CPW filters using coupled metamaterial resonators[J]. *IEEE Trans. Microw. Theory Tech*, 2006, **54**(6): 2628 - 2635.
[8] Paul O, Beigang R, Rahm M. Highly selective terahertz bandpass filters based on trapped mode excitation[J]. *Opt. Express*, 2009, **17**(21): 18590 - 18595.
[9] Chin J Y, Lu M, Cui T J. Metamaterial polarizers by electric-field-coupled resonators[J]. *Appl. Phys. Lett*, 2008, **93**: 251903 - 251905.
[10] Wei X, Shi H, Dong X, *et al*. A high refractive index metamaterial at visible frequencies formed by stacked cut-wire plasmonic structures[J]. *Appl. Phys. Lett*, 2010, **97**(1): 011904 - 011907.
[11] Smith D R, Schultz S, Markos P, *et al*. Determination of effective permittivity and permeability of metamaterials from reflection and transmission coefficients[J]. *Phys. Rev. B*, 2002, **65**: 195104 - 195108.
[12] Hua Y L, Li Z Y. Analytic modal solution to transmission and collimation of light by one-dimensional nanostructured subwavelength metallic slits[J]. *J. Appl. Phys*, 2009, **105**: 013104 - 013111.
[13] Smith D R, Vier D C, Konschny T, *et al*. Electromagnetic parameter retrieval from inhomogeneous metamaterials[J]. *Phys. Rev. E*, 2005, **71**: 036617 - 036627.
[14] Fernaćndez-Domìnguez A I, Martin-Moreno L, Garcia-Vidal J, *et al*. Spoof surface plasmon polariton modes propagating along periodically corrugated wires[J]. *IEEE J. Sel. Top. Qantum Electron*, 2008, **14**(6): 1515 - 1521.